

Gas expulsion vs gas retention in young stellar clusters II: effects of cooling and mass segregation

Sergiy Silich ^{*} and Guillermo Tenorio-Tagle

Instituto Nacional de Astrofísica Óptica y Electrónica, AP 51, 72000 Puebla, México

Accepted XXX. Received YYY; in original form ZZZ

ABSTRACT

Gas expulsion or gas retention is a central issue in most of the models for multiple stellar populations and light element anti-correlations in globular clusters. The success of the residual matter expulsion or its retention within young stellar clusters has also a fundamental importance in order to understand how star formation proceeds in present-day and ancient star-forming galaxies and if proto-globular clusters with multiple stellar populations are formed in the present epoch. It is usually suggested that either the residual gas is rapidly ejected from star-forming clouds by stellar winds and supernova explosions, or that the enrichment of the residual gas and the formation of the second stellar generation occur so rapidly, that the negative stellar feedback is not significant. Here we continue our study of the early development of star clusters in the extreme environments and discuss the restrictions that strong radiative cooling and stellar mass segregation provide on the gas expulsion from dense star-forming clouds. A large range of physical initial conditions in star-forming clouds which include the star-forming cloud mass, compactness, gas metallicity, star formation efficiency and effects of massive stars segregation are discussed. It is shown that in sufficiently massive and compact clusters hot shocked winds around individual massive stars may cool before merging with their neighbors. This dramatically reduces the negative stellar feedback, prevents the development of the global star cluster wind and expulsion of the residual and the processed matter into the ambient interstellar medium. The critical lines which separate the gas expulsion and the gas retention regimes are obtained.

Key words: galaxies: star clusters — Globular Clusters — Physical Data and Processes: hydrodynamics

1 INTRODUCTION

Globular clusters (GCs), considered for a long time to be chemically homogeneous stellar systems are now confirmed to have distinct stellar subpopulations with different He contents, different abundances of light elements and well documented anti-correlations between elements such as O and Na, Mg and Al (see [Bedin et al. 2004](#); [Gratton et al. 2004](#); [Marino et al. 2008](#); [Carretta et al. 2009](#); [Piotto et al. 2012](#); [Cabrera-Ziri et al. 2015](#); [Renzini et al. 2015](#), and references therein). It has been proposed that the first generation of stars (1G) is formed from the pristine (unpolluted) matter whereas the second (2G) and in some cases subsequent stellar generations originate from the leftover gas or from accreted primordial matter enriched with the high temperature hydrogen burning products produced by the 1G stars (see [Gratton et al. 2004](#); [Prantzos & Charbonnel 2006](#);

[Decressin et al. 2007](#); [D’Ercole et al. 2008](#); [de Mink et al. 2009](#); [Renzini et al. 2015](#); [Elmegreen 2017](#), and references therein). A strong constraint on the multiple populations models is that most GCs with the exception of the most massive ones are homogeneous in iron-peak elements (see [Renzini 2013](#), and references therein). This implies that pollution of the pristine gas is not caused by the 1G SN explosions and this leads to two major pollution scenarios - fast, and slow.

In the slow pollution scenario stellar winds formed by massive stars and SN explosions expel the residual gas from the cluster. Intermediate mass AGB stars then shed processed gas at low velocity. The enriched matter is accumulated in the gravitational well of the cluster and mixes with primordial gas accreted later from the ambient medium. The 2G of stars then results from this polluted matter (e.g. [D’Ercole et al. 2008, 2010](#); [Conroy & Spergel 2011](#)).

In the fast pollution scenario it is suggested that the 2G stars are formed from the matter polluted within

* E-mail: silich@inaoep.mx

a short time-scale either by fast rotating massive stars (Prantzos & Charbonnel 2006; Decressin et al. 2007) or by interacting massive binaries (de Mink et al. 2009). In different versions of this scenario it has been suggested that proto-stellar discs sweep up matter enriched by fast rotating massive stars or interacting massive binaries (Early Disc Accretion Model Bastian et al. 2013; Cassisi & Salaris 2014). Other authors have proposed that fast rotating massive stars form slow winds and trigger the 2G formation in their vicinity (Decressin et al. 2007), or that pollution occurs due to interactions between massive stars in very dense stellar clusters (Elmegreen 2017). In the rapidly cooling star cluster wind model by Wünsch et al. (2017) dense enriched clumps are formed in the central zones of thermally unstable star cluster winds. They then self-shield against the ionizing photons and accumulate inside the cluster to form the 2G of stars before massive stars begin to explode as SNe.

Gas expulsion or gas retention is a central issue in all of these models. It is also crucial in order to understand how stellar feedback affects the residual gas in young present-day clusters and in those formed in assembling galaxies and if proto-globular clusters with multiple stellar populations can be formed at the present epoch.

There is a common belief that negative feedback provided by massive stars rapidly clears out star-forming regions from the residual gas and that this process acquires even larger importance in denser, more compact clusters with smaller mean separations between neighboring stars (e.g. Krause et al. 2012). In most multiple populations models the negative stellar feedback either is not discussed, or it is assumed that it results in a star cluster wind. The full 3D numerical simulations by Calura et al. (2015) seem to confirm these expectations.

Recent attempts to find the residual gas in present-day young massive clusters did not reveal any significant amount of gas (see Bastian et al. 2013, 2014). However observations in radio, IR and recently in the sub-millimeter regime have revealed several very bright, optically obscured objects which are believed to be massive, very compact star clusters still embedded into their natal star-forming clouds (Turner et al. 2000; Gorjian et al. 2001; Turner et al. 2003; Beck et al. 2012; Whitmore et al. 2014; Beck 2015; Turner et al. 2015; Consiglio et al. 2016; Turner et al. 2017; Oey et al. 2017). It is not clear so far if in these cases we witness the earliest stages of massive clusters assembling as it is often suggested in the case of the still enshrouded clusters, or if the negative star formation feedback is in these cases strongly suppressed by the high-pressure environment or by in-falling gas filaments (see the discussion in Martín-Hernández et al. 2005; Silich et al. 2007; Whitmore et al. 2014; Matzner & Jumper 2015; Calzetti et al. 2015; Smith et al. 2016; Silich & Tenorio-Tagle 2017; Consiglio et al. 2017).

This led us to discuss the impact that turbulent pressure and strong radiative cooling provide on the gas expulsion from clusters formed under extreme conditions. In Silich & Tenorio-Tagle (2017, paper I) we have shown that in very massive and compact clusters wind-driven shells around individual massive stars do not merge, suppressing the development of a global star cluster wind. Here we discuss the post-stalling hot shocked gas evolution. It is shown that hot shocked gas zones around individual massive stars then grow

in the subsonic regime until they merge with hot bubbles produced by neighboring massive stars or until catastrophic cooling sets in and the shocked gas becomes thermally unstable. A global star cluster wind that expels the residual gas from the star-forming region is formed in the former case, whereas in the latter case the negative stellar feedback is strongly suppressed, hot shocked zones around individual stars do not merge and the star cluster wind is not formed. The critical lines which separate stellar clusters which expel or retain the residual gas and the matter returned by massive stars are derived. We also discuss how the initial mass segregation affects the critical lines.

We consider instantaneous star formation and depart from the basic assumption that stellar winds are synchronized and continuous while SNe do not coincide either in space or time. Therefore we do not examine the effects of SNe explosions assuming that the supernovae products blow away from clusters providing little effect on the leftover gas distribution (Tenorio-Tagle et al. 2015) or that most massive stars do not explode, but collapse directly into black holes as has been argued by other authors (see Decressin et al. 2010; Adams et al. 2017a,b; Mirabel 2017a,b, and references therein).

The paper is organized as follows: in section 2 we discuss the stellar and gas density distribution in star-forming molecular clouds, used later on for our numerical calculations. Here we also present the adopted global and individual stellar wind energy and mass lost rate. In section 3 the distributions of pressure, density, temperature and expansion velocity in the pressure-confined shocked wind zones around individual stars are obtained by solving the set of the steady state spherically-symmetric hydrodynamic equations numerically. It is demonstrated that in dense, compact clusters hot shocked winds may cool down before merging with their neighbors. In section 4 the results from these simulations are used to build critical lines which separate clusters which are able to retain all gas, which includes the residual gas and that reinserted by massive stars, from those which form global star cluster winds, clear their star-forming clouds and expel all gas into the ambient interstellar medium. Our major results are summarized in Section 5.

2 MODEL SETUP

2.1 The star-forming cloud model

Following recent papers (e.g. Krause et al. 2012; Calura et al. 2015; Silich & Tenorio-Tagle 2017) we consider star-forming clouds with a Plummer density distribution:

$$\rho_g(r) = \frac{3(1-\epsilon)M_{tot}}{4\pi a^3} \left(1 + \frac{r^2}{a^2}\right)^{-5/2}, \quad (1)$$

$$\rho_*(r) = \frac{3\epsilon M_{tot}}{4\pi a^3} \left(1 + \frac{r^2}{a^2}\right)^{-5/2}, \quad (2)$$

where $\rho_g(r)$ and $\rho_*(r)$ are the gas and the stellar mass density distribution, respectively, M_{tot} is the initial mass of the star-forming cloud and ϵ is the star formation efficiency. In the case of a Plummer density distribution the half-mass radius is $R_{hm} = 1.3a$, where a is the characteristic length

scale or the core radius of the star-forming cloud. The pressure profile in such a cloud is determined by the equation of the hydrostatic equilibrium (Calura et al. 2015):

$$\frac{dP_g}{dr} = -\frac{GM(r)\rho_g(r)}{r^2}, \quad (3)$$

where G is the gravitational constant and the total mass $M(r)$ enclosed within a sphere of radius r is:

$$M(r) = \frac{r^3 M_{tot}}{(r^2 + a^2)^{3/2}}. \quad (4)$$

One can integrate equation (3) and obtain the distribution of the gas pressure in the star-forming cloud:

$$P_g(r) = \frac{(1-\epsilon)GM_{tot}^2}{8\pi a^4} \left(1 + \frac{r^2}{a^2}\right)^{-3} + C, \quad (5)$$

where C is the integration constant. Hereafter we assume that at large distances from the cloud center the gas pressure goes to zero and therefore $C = 0$. Given the low temperature of the molecular gas, it is likely that the intra-cluster gas pressure is dominated by turbulence (Elmegreen & Efremov 1997; Elmegreen 2017; Johnson et al. 2015). In this case $P_g = \rho_g \sigma^2$ (e.g. Smith et al. 2006), where the one-dimensional velocity dispersion σ is:

$$\sigma^2 = \frac{GM_{tot}}{6a} \left(1 + \frac{r^2}{a^2}\right)^{-1/2}. \quad (6)$$

The distribution of gas pressure, density and velocity dispersion σ in a $M_{tot} = 10^6 M_\odot$ star-forming clouds with a star formation efficiency $\epsilon = 0.3$ and different core radii is shown in Fig. 1. One can note that the central gas density strongly depends on the cloud compactness. It is much larger in clouds with smaller core radii (see panel a in Fig. 1) as in this case the same mass is concentrated in a smaller volume. This results in a stronger gravitational pull and a larger gas central pressure (see panel b in Fig. 1). It is likely that precursors of globular clusters were formed in a high pressure environment and that this led to their compactness and to a large star formation efficiency required to form bound, long-lived clusters (see Ashman & Zepf 2001, and references therein).

Hereafter it is assumed that due to primordial mass segregation all massive stars are concentrated within the central zone of the star-forming cloud (Baumgardt et al. 2008; Dib et al. 2008). The number of massive stars per unit volume then is:

$$N(r) = \frac{3N_*(t)}{4\pi R_{sg}^3} \left(1 + \frac{R_{sg}^2}{a^2}\right)^{3/2} \left(1 + \frac{r^2}{a^2}\right)^{-5/2} \quad r < R_{sg}, \quad (7)$$

$$N(r) = 0 \quad r > R_{sg}, \quad (8)$$

where $N_*(t)$ is the total number of massive stars in the cluster and R_{sg} is the radius of the mass-segregation zone. In this case the mean separation between nearby massive stars $\Delta = 2X$, where the half-distance between neighboring sources is:

$$X = R_{sg} \left(1 + \frac{R_{sg}^2}{a^2}\right)^{-1/2} \left(1 + \frac{r^2}{a^2}\right)^{5/6} N_*(t)^{-1/3}. \quad (9)$$

When the mass segregation radius $R_{sg} \rightarrow \infty$, relation (9) reduces to that obtained in Silich & Tenorio-Tagle (2017), their equation (4). In the case of a standard Kroupa initial

mass function (IMF) the initial number of single massive ($M > 8 M_\odot$) stars $N_*(0)$ in an instantaneous stellar cluster scales with the star cluster mass as (e.g. Calura et al. 2015):

$$N_*(0) = N_0(M_*/10^6 M_\odot), \quad (10)$$

where $N_0 = 10^4$, $M_* = \epsilon M_{tot}$. Note, that the number of massive stars $N_*(t)$ drops whereas the mean separation between neighboring massive stars grows after the onset of supernova explosions. At this stage

$$N_*(t) = N_*(0) - E_{SN}/E_0, \quad (11)$$

where E_{SN} is the total energy of SN explosions calculated by means of Starburst99 synthetic model (Leitherer et al. 1999) and $E_0 = 10^{51}$ erg is the energy of each supernova explosion.

It is assumed that the star formation efficiency ϵ is the same at all radii. The possible growth of the star formation efficiency in the central zone of the star-forming cloud is not considered, but is expected to be qualitatively similar to the influence of mass segregation.

2.2 The stellar wind energy

Fig. 2 presents the time evolution of the stellar winds cumulative mechanical luminosity, mass loss rate and the number of massive stars in an instantaneous $10^6 M_\odot$ cluster with a standard Kroupa IMF and Padova stellar evolutionary tracks with AGB stars predicted by the Starburst99 version 7. The solid and dotted lines in Fig. 2 display the mechanical luminosity, the stellar mass loss rate and the number of massive stars in clusters with $Z = Z_\odot$ and $Z = 0.02Z_\odot$ metallicity, respectively. Note that low metallicity clusters are much less energetic and return less mass into the ambient medium. Hereafter it is assumed that all massive stars are identical. The Starburst99 model together with equation (10) then allow one to obtain the mechanical luminosity L_* and the mass loss rate \dot{M}_* of a typical massive star at any time t . During the first 10 Myr the mechanical luminosities of individual stellar winds change within the range $2 \times 10^{34} \leq L_* \leq 2 \times 10^{36}$ erg s⁻¹ in clusters with solar abundances and $3 \times 10^{33} \leq L_* \leq 4 \times 10^{35}$ erg s⁻¹ in clusters with $Z = 0.02Z_\odot$, respectively, to become negligible after 10 Myr.

3 SHOCKED WIND BUBBLES IN A HIGH PRESSURE INTRA-CLOUD MEDIUM

Each massive star produces a fast stellar wind which is heated up at a reverse shock and drives a leading shock into the ambient medium. The leading shock sweeps up the ambient gas into a dense narrow shell which, at first, expands supersonically. In paper I we found the critical densities required for the wind-driven shells to stall before merging. This occurs when the pressure in the hot, shocked wind drops to that in the turbulent ambient medium. The wind-driven shell expansion velocity then drops below the intra-cloud gas turbulent speed and it begins to disintegrate due to Rayleigh-Taylor instabilities and perturbations provided by the ambient gas. However, the hot, shocked wind zone continuous to grow even after the wind-driven shell stalls as the central star continues to deposit mass and energy for a much longer time. The hot shocked wind zone grows then in

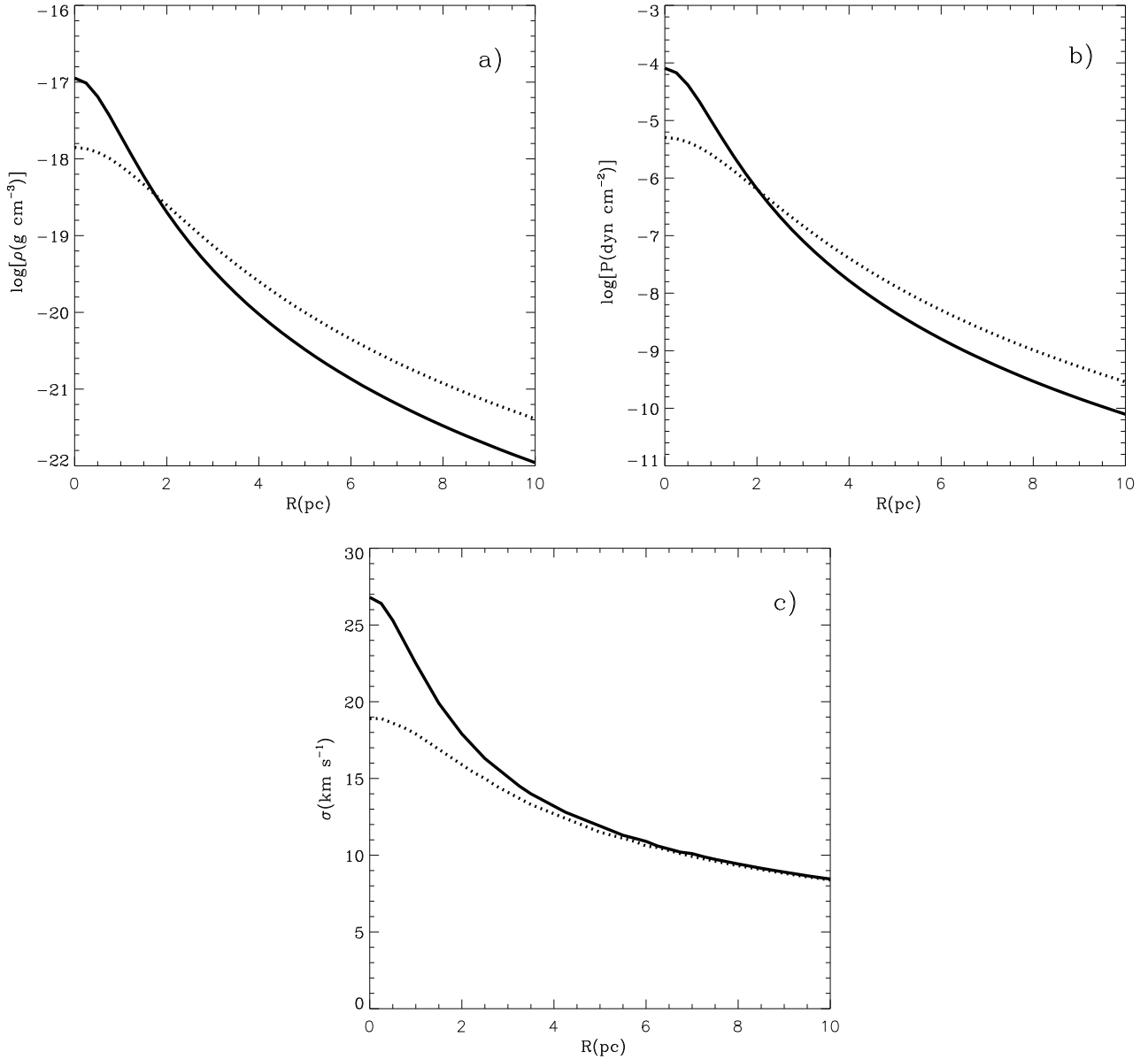


Figure 1. The distribution of the gas density (panel a), pressure (panel b) and one dimensional velocity velocity dispersion (panel c) in a star-forming cloud. The solid and dotted lines correspond to $10^6 M_{\odot}$ clouds with star formation efficiency $\epsilon = 0.3$ and core radii $a = 1\text{pc}$ and $a = 2\text{pc}$, respectively.

the subsonic regime (see Appendix A) until it merges with a neighboring hot shocked wind or reaches its cooling radius and catastrophic gas cooling sets in. During the evolution the stellar wind is heated up at the reverse shock whose radius R_{RS} is determined by the condition that the stellar wind ram pressure is equal to the pressure in the turbulent ambient medium:

$$R_{RS} = \frac{a^2}{M_{tot}} \left[\frac{4L_{\star}}{(1-\epsilon)GV_{\star}} \right]^{1/2} \left(1 + \frac{R^2}{a^2} \right)^{3/2}, \quad (12)$$

where $V_{\star} = (2L_{\star}/\dot{M}_{\star})^{1/2}$ is the stellar wind terminal speed. One can determine how the gas temperature, density and pressure are distributed in the slowly growing, subsonic shocked wind zones by making use of steady state, spher-

ically symmetric hydrodynamic equations which include the gas cooling term (e.g. [Silich et al. 2004](#)):

$$\frac{1}{r^2} \frac{d\rho u r^2}{dr} = 0, \quad (13)$$

$$\rho u \frac{du}{dr} = -\frac{dP}{dr}, \quad (14)$$

$$\frac{1}{r^2} \frac{d}{dr} \left[\rho u r^2 \left(\frac{u^2}{2} + \frac{\gamma}{\gamma-1} \frac{P}{\rho} \right) \right] = -Q, \quad (15)$$

where $Q = n_i n_e \Lambda(T, Z)$ is the cooling rate, $\Lambda(T, Z)$ is the Raymond et al. cooling function ([Raymond et al. 1976](#)), $n_i \approx n_e$ are the ion and electron densities in the hot shocked wind and Z is the stellar wind metallicity. One

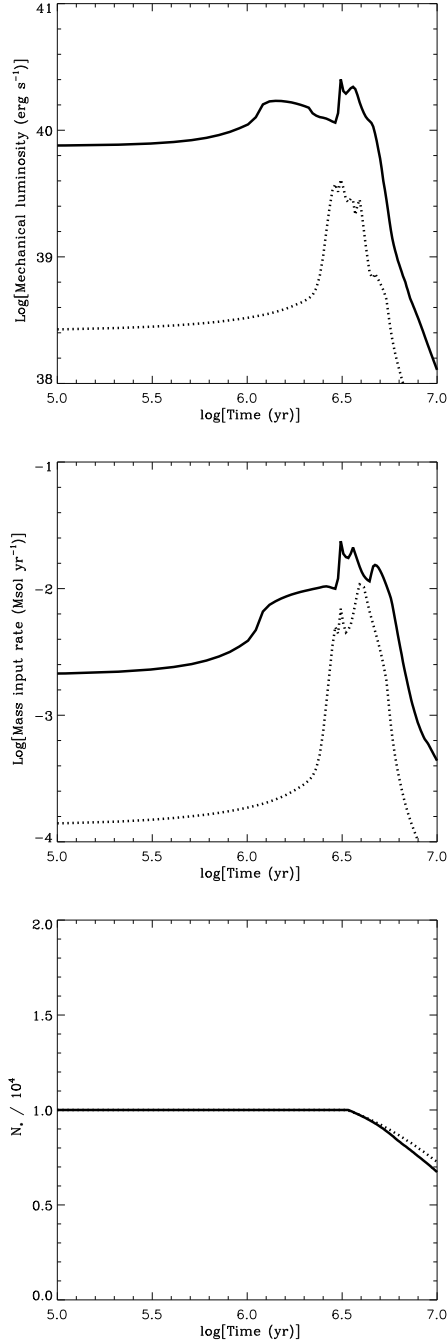


Figure 2. Total mechanical luminosity and mass loss rate of stellar winds and the number of massive stars in a $10^6 M_\odot$ stellar cluster. The mechanical luminosity L_{SC} and the stellar mass loss rate \dot{M}_{SC} were calculated by means of the Starburst99, version 7 with Padova stellar evolutionary tracks which includes AGB stars. The number of massive stars was scaled with the star cluster mass and the total energy of SNe. The solid and dotted lines show the results of the calculations for clusters with $Z = Z_\odot$ and $Z = 0.02Z_\odot$, respectively.

can integrate equation (13) and present the set of equations (13)-(15) in a form suitable for the numerical integration:

$$\frac{du}{dr} = \frac{1}{r\rho} \frac{(\gamma - 1)rQ + 2\gamma uP}{u^2 - c^2}, \quad (16)$$

$$\frac{dP}{dr} = -\rho u \frac{du}{dr}, \quad (17)$$

$$\rho = \frac{\dot{M}_*}{4\pi ur^2}, \quad (18)$$

where $c^2 = \gamma P/\rho$ is the sound speed in the shocked wind plasma. The temperature of the shocked wind is $T = \mu_i c^2/\gamma k$, where $\mu_i = 14/23m_H$ is the mean mass per particle in the completely ionized gas with 1 helium atom per each 10 hydrogen atoms, m_H is the mass of the hydrogen atom and k is the Boltzmann constant. The set of equations (16) - (18) should be integrated numerically outwards from the reverse shock location. The initial conditions for the numerical integration (the values of the shocked wind density, ρ_{sw} , temperature, T_{sw} , and pressure, P_{sw} behind the reverse shock) are determined by the Rankine-Hugoniot conditions:

$$\rho_{sw} = \frac{\gamma + 1}{\gamma - 1} \rho_w(R_{RS}) = \frac{\gamma + 1}{\gamma - 1} \frac{(1 - \epsilon)GM_{tot}^2}{8\pi a^4 V_*^2} \left(1 + \frac{r^2}{a^2}\right)^{-3} \quad (19)$$

$$T_{sw} = \frac{2(\gamma - 1)}{(\gamma + 1)^2} \frac{\mu_i}{k} V_*^2, \quad (20)$$

$$P_{sw} = \frac{2(\gamma - 1)}{(\gamma + 1)^2} \rho_{sw} V_*^2, \quad (21)$$

$$V_{sw} = \frac{\gamma - 1}{\gamma + 1} V_*. \quad (22)$$

The results of the numerical integration in the case of a $3 \times 10^5 M_\odot$, 1 Myr old cluster with $R_{sg} = a$, formed in a $10^6 M_\odot$ cloud with metallicity $Z = 0.02Z_\odot$, are presented in Fig. 3. Here the dashed, solid and dotted lines display the distribution of the hydrodynamical variables in the subsonic shocked wind zone around an individual massive star when it is located in the center of clusters with different core radii (2 pc, 3 pc and 4 pc, respectively). Vertical lines indicate the half distance between neighboring massive stars in each of these cases. The gas, whose speed behind the reverse shock is equal to one quarter of the stellar wind terminal speed (in this case $V_* = 2370 \text{ km s}^{-1}$), rapidly slows down (see panel a) because of the inverse thermal pressure gradient in the shocked wind zone. When the velocity of the gas becomes negligible and its ram pressure vanishes, the thermal pressure reaches a balance with the ambient gas pressure and remains homogeneous throughout the shocked wind zone (see panel b). In the case of the less compact cloud (dotted lines in Fig. 3), the impact of radiative cooling is negligible. In this case the density and the temperature in the shocked wind zone do not change significantly and the shocked wind remains hot as it merges with a neighboring shocked wind bubble (see dotted lines on panels c and d). Neighboring hot bubbles then fill in the whole star-forming region and form a star cluster wind able to expel all gas, which includes the residual and that reinserted by massive stars, from the star cluster volume. Such clusters are not able to form a second stellar generation unless they further accrete a sufficient amount of matter. One can estimate the characteristic time

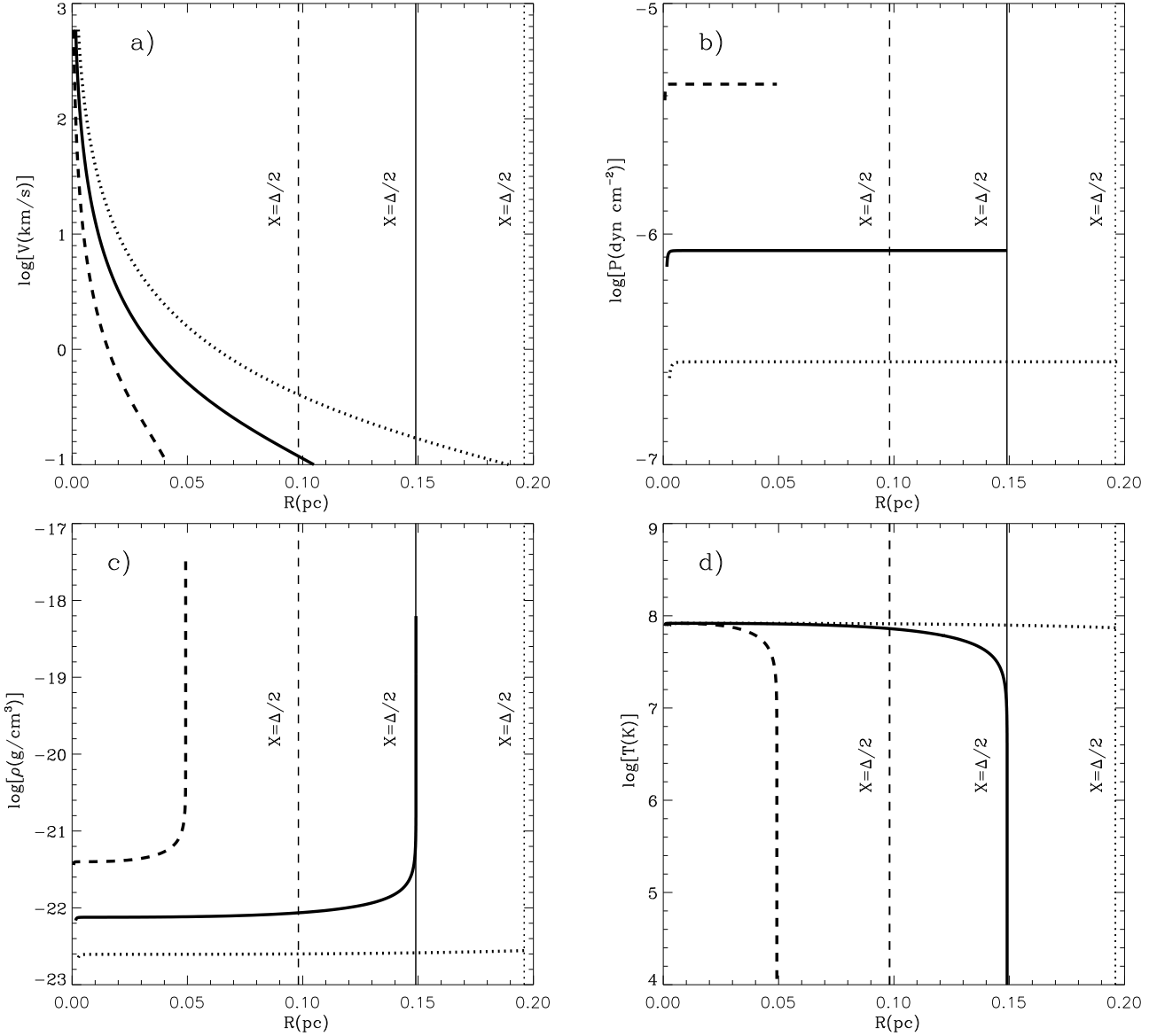


Figure 3. The distribution of the gas temperature, velocity, density and pressure in the shocked wind zone around individual stars located in the center of a dense star-forming cloud. The calculations were provided for a 1 Myr old, $3 \times 10^5 M_{\odot}$ cluster formed in a $10^6 M_{\odot}$ cloud with low metallicity $Z = 0.02 Z_{\text{sol}}$ and $R_{\text{sg}} = a$. The dashed, solid and dotted lines display the distribution of the expansion velocity (panel a), thermal pressure (panel b), density (panel c) and temperature (panel d) in the shocked wind zone around individual stars in the case when the cluster is formed in clouds with different core radii: $a = 2 \text{ pc}$, $a = 3 \text{ pc}$ and $a = 4 \text{ pc}$, respectively. The vertical dashed, solid and dotted lines show the mean half distance between neighboring massive stars in each case.

τ_w , which is required for hot bubbles to merge in such clusters, by integrating equation (A5) from Appendix A. This time depends on the location of the neighboring stars in the cluster. In the case of a $3 \times 10^5 M_{\odot}$ cluster with a core radius $a = 4 \text{ pc}$ (dotted lines in Fig. 3), $\tau_w \approx 8 \times 10^5 \text{ yr}$ when stars are located near the star cluster center and $\tau_w \approx 6 \times 10^5 \text{ yr}$ when they are located at the edge of the mass segregation zone. Thus, in this case it takes less than 1 Myr for massive stars to fill in the star forming region with a hot gas and form a cluster wind similar to that suggested by Chevalier & Clegg (1985).

However, in more compact or more massive clusters radiative cooling becomes a dominant factor. In such clusters the gas velocity in the shocked wind zone behind the reverse

shock also drops rapidly and thermal pressure reaches a balance with the pressure in the ambient intra-cluster medium (see solid and dashed lines in panels a and b). However, stellar winds heated at the reverse shocks behave adiabatically only in a narrow zone behind the shock. At larger distances radiative losses become important. The shocked gas temperature begins to deviate from the post-reverse shock value and drops dramatically when the gas in the shocked wind zone becomes thermally unstable (see dashed and solid lines on panel d). The shocked wind density increases then orders of magnitude (see panel c) to sustain pressure balance, and dense molecular clumps are formed. This results in a dynamical, multi-phase intra-cluster medium where hot gas is confined to small compact bubbles around individual stars

and co-exists with partially photo-ionized residual gas and dense clumps resulting from the thermally unstable reinserted matter as also occurs in the inner zones of thermally unstable star cluster winds (e.g. Wünsch et al. 2009).

Note, that in clusters which are not sufficiently compact or massive, the shocked winds may cool before merging if they are in the central zone of the cluster, but merge at the edge of the mass segregation zone, as is the case in the $3 \times 10^5 M_{\odot}$ clusters with core radii 2 pc and 3 pc where the shocked winds cool before merging in the center (see Fig. 3), but not at the edge of the mass segregation zone. Hot shocked bubbles never merge if the hot shocked gas cools catastrophically at half the distance or smaller between neighboring stars located at the edge of the mass segregation zone. The negative stellar feedback in such clusters is dramatically reduced. The hot gas occupies only a fraction of the star-forming volume and is not able to escape from the potential well of the cluster and form a cluster wind. In such clusters the leftover gas may mix with the cool reinserted matter and form another generation of stars with a different chemical composition.

The critical star-forming cloud size is determined then by the condition that the shocked wind gas at the edge of the mass segregation zone cools down exactly at the half distance between neighboring sources. The critical half-mass radius R_{crit} of the cluster depends on the mass of the star-forming cloud, the star formation efficiency, the natal gas metallicity and on the concentration of massive stars towards the star cluster center (on the value of the mass segregation radius R_{sg}). It also depends on the evolutionary time t as the stellar mechanical luminosity, the mass loss rate and the number of massive stars change with time (see Fig. 2). One can obtain the value of R_{crit} by iterating the star-forming cloud core radius in the initial conditions (19) - (22) and integrating the set of the hydrodynamic equations (16) - (18) numerically until the shocked gas at the edge of the mass segregation zone cools exactly at the half distance between neighboring sources. The critical half-mass radii calculated at different times for proto-stellar clouds with masses $10^5 M_{\odot}$, $10^6 M_{\odot}$ and $10^7 M_{\odot}$ (dotted, solid and dashed lines, respectively) assuming a star formation efficiency $\epsilon = 0.3$ and metallicity $Z = 0.02Z_{\odot}$ are shown in Fig. 4.

R_{crit} reaches the minimum value R_{min} just before the onset of SN explosions, when the stellar winds power reaches the maximum value (see Fig. 2). After the beginning of SN explosions the critical half-mass radius increases rapidly because the power of stellar winds drops and the mean separation between massive stars grows. Clusters whose radii are smaller than R_{min} retain the residual and the reinserted matter whereas those with $R_{hm} > R_{min}$ form hot star cluster winds.

4 CATASTROPHIC COOLING VERSUS THE RESIDUAL GAS EXPULSION

4.1 The critical size of the star-forming cloud and the critical gas central density

One can now use the procedure described in the previous section to calculate the critical half-mass radius at successive

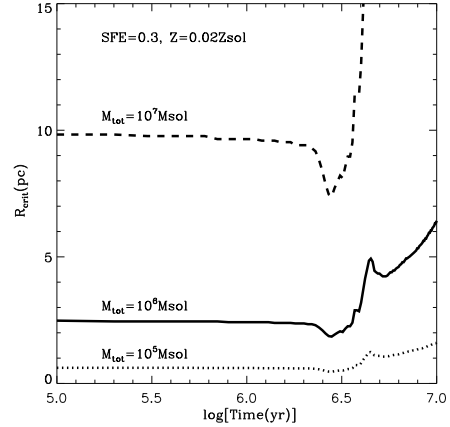


Figure 4. The star-forming cloud critical half-mass radii. The calculations were provided for star-forming clouds with $10^5 M_{\odot}$, $10^6 M_{\odot}$ and $10^7 M_{\odot}$ proto-stellar clouds with star formation efficiency $\epsilon = 0.3$, metallicity $Z = 0.02Z_{\odot}$ and the mass segregation radius equal to the star-forming cloud core radius, $R_{sg} = a$.

evolutionary times t and select the minimum half-mass radius from those calculated at different star cluster ages. This determines the critical half-mass radius $R_{hm,crit} = R_{min}$ of the star-forming cloud and its emerging cluster. Clusters whose radii are smaller than $R_{hm,crit}$ are not able to form a cluster wind and expel gas from the star-forming cloud whereas those whose radii are larger than $R_{hm,crit}$ form hot winds which clean up the cluster from the residual and the reinserted matter.

Critical lines which separate clusters that retain gas and those which form cluster winds are shown in Fig. 5. Here the results of the calculations for clouds with solar $Z = Z_{\odot}$ and $Z = 0.02Z_{\odot}$ abundances are shown in the left and right panels, respectively. The mass segregation radius selected for these calculations is equal to the star cluster core radius: $R_{sg} = a$. The solid and dashed lines show the critical lines calculated for star formation efficiencies $\epsilon = 0.2$ and $\epsilon = 0.5$, respectively, which are often suggested as lower and upper limits for the star formation efficiency in proto-globular clusters (Ashman & Zepf (2001); Kroupa et al. (2001); Johnson et al. (2015)). The upper panels show the critical half-mass radii, whereas the bottom ones the critical gas central densities. One can notice, that star-forming clouds must be sufficiently massive in order to be located in the gas retention parameter space and have central gas densities which do not exceed the maximum stellar mass and molecular gas density ($\sim 10^7 \text{ cm}^{-3}$, the horizontal dotted lines in Fig. 5) so far detected in globular clusters and Galactic molecular clouds (see Renzini 2013; Rathborne et al. 2015). This may explain observational constraints on the low mass limit for stellar clusters with multiple stellar populations (see Carretta et al. 2010; Salinas & Strader 2015; Mucciarelli et al. 2016; Massari et al. 2017, and references therein). It is also remarkable that the critical half-mass radii required for the gas retention (see upper panels in Fig. 5) are close to those of globular clusters (Ashman & Zepf 2001; Johnson et al. 2015).

A comparison of the left and right panels in Fig. 5 also

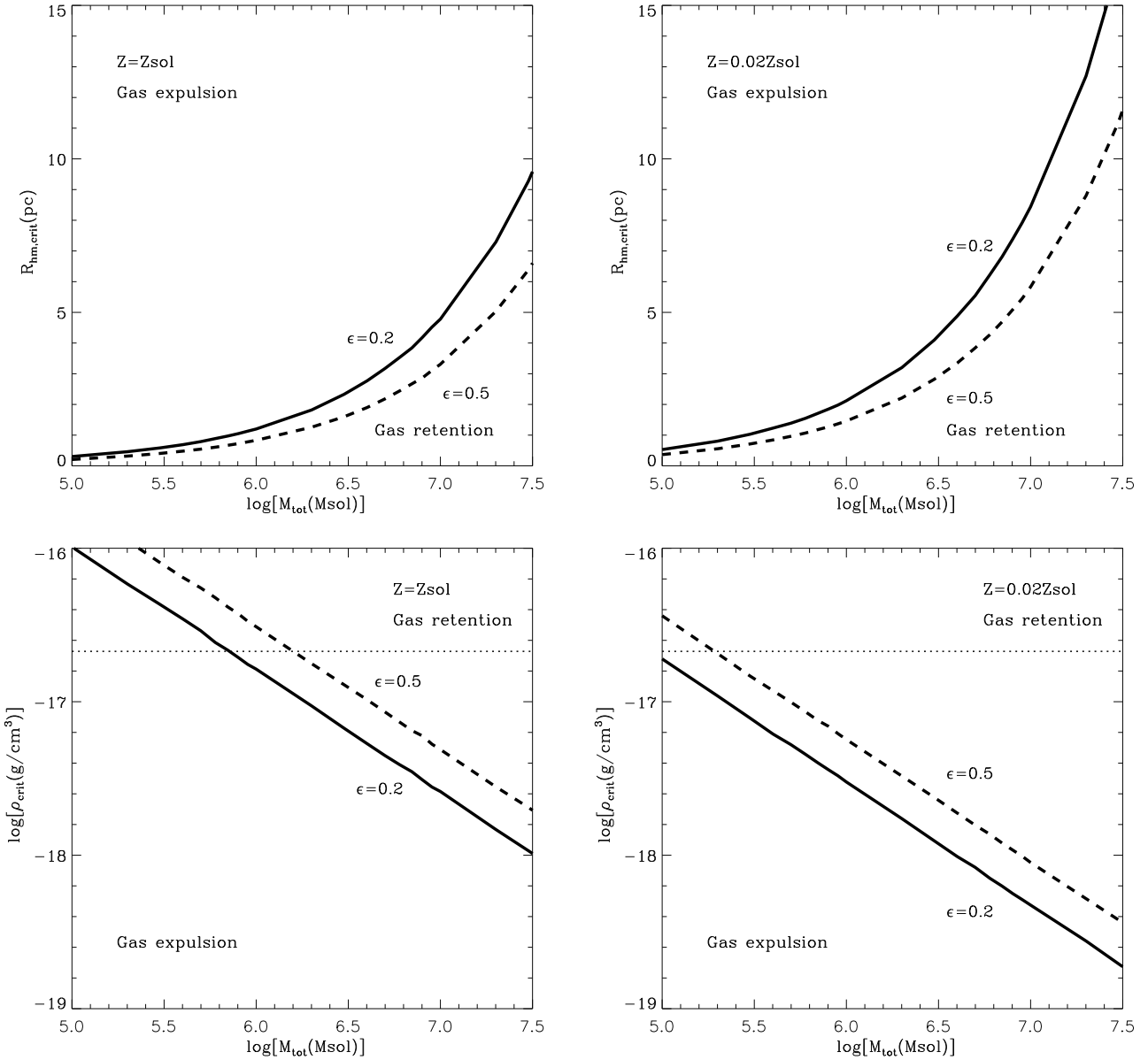


Figure 5. Star-forming clouds critical radii and gas central densities. The left-hand and right-hand panels present the results of the calculations for star-forming clouds with solar and $Z = 0.02Z_{\odot}$ abundances. The upper and bottom panels display the critical half-mass radii and gas central densities, respectively. The solid and dashed lines correspond to star-forming clouds with different star formation efficiencies, $\epsilon = 0.2$ and $\epsilon = 0.5$, respectively. The dotted lines on the bottom panels mark the largest stellar mass density detected in globular clusters. Clusters located below the critical lines on the top panels or above the critical lines on the bottom panels retain the leftover gas after the 1G formation whereas clusters located above the threshold lines on the top panels and below the threshold lines on the bottom panels rapidly form star cluster winds.

shows that clusters formed in present day galaxies must be more massive and compact than young proto-globular clusters formed from pristine matter with a low metal content in order to retain gas within the star-forming volume. Therefore the window of opportunity to form a 2G of stars is larger in the case when star formation occurs in low metallicity clouds.

Fig. 5 also illustrates the significant role of the star formation efficiency for the success of gas retention or expulsion from the natal star-forming cloud. Indeed, the star-forming

cloud location on Fig. 5 depends not only on the star cluster mass and compactness, but also on the star formation efficiency which determines the amount of gas left over from the 1G formation.

4.2 Effects of mass segregation

In order to examine how the concentration of massive stars towards the star cluster center affects the critical lines, we calculated the critical radii and gas central densities for

star-forming clouds with different mass segregation radii: $R_{sg} = a$, $R_{sg} = 2a$ and $R_{sg} = a/2$. The results of the calculations are presented in Fig. 6. Critical radii and densities do not change significantly in the case when the mass segregation radius is smaller than the star cluster core radius, $R_{sg} < a$ (compare the solid and dotted lines in Fig. 6). However, in the case when $R_{sg} > a$ (dashed lines in Fig. 6), the difference is notable. The impact of the mass segregation zone size on the threshold lines in these two cases is different because the ambient gas density and the gas pressure in the central zone of the cloud ($r < a$) do not change so rapidly as they do in the outer zone (see Fig. 1). In clusters with $R_{sg} < a$ reverse shocks around massive stars at the edge of the mass segregation zone have smaller radii than in the case when $R_{sg} = a$ as the intra-cloud gas pressure grows towards the center. This results in larger densities and faster gas cooling in the shocked wind zones. Therefore in the case when $R_{sg} < a$ catastrophic gas cooling occurs in clusters with larger half-mass radii than in the case when $R_{sg} = a$. The difference between the critical lines in this case is negligible as the pressure gradient in the central zone of the star-forming cloud is small. In clusters with $R_{sg} > a$ the ambient gas pressure at the edge of the mass segregation zone is smaller than in clusters with $R_{sg} = a$. Therefore reverse shocks are located further away from their stars and star-forming clouds must be more compact in order that shocked winds cool before merging with their neighbors. In this case the difference between the critical lines is significant as the intra-cloud pressure drops rapidly outside of the central zone and the star-forming cloud must be much more compact than in the case when $R_{sg} = a$ in order the shocked winds at the edge of the mass segregation zone cool before merging with their neighbors. The triangle symbol in Fig. 6 marks the initial gas central density used by Calura et al. (2015) in their 3D numerical simulations. One can note that clouds with such star formation efficiency ($\epsilon = 0.3$) and such gas central densities ($\sim 5 \times 10^3 \text{ cm}^{-3}$) are located in the gas expulsion parameter space, far away from the critical lines. Thus the conclusion made by Calura et al. (2015) who claimed that stellar winds remove the residual gas from such star-forming cloud is in agreement with our findings.

4.3 Star cluster compactness and critical star formation efficiency

Top panels in Fig. 5 and Fig. 6 also show that only sufficiently compact clusters are able to retain the leftover and the reinserted matter. The crucial role of the cluster compactness was also stressed by Krause et al. (2016) who introduced the star cluster compactness index $C_5 = (M_{SC}/10^5 M_\odot)/(R_{hm}/1 \text{ pc})$ and concluded that this index together with star formation efficiency completely determine the success of the gas expulsion from the star-forming cloud (see their Fig. 4).

In our model the compactness of star-forming clouds is also important. However the critical efficiency depends not only on the compactness index, but also on the star cluster mass. The critical star formation efficiencies calculated for clusters with Z_\odot and $0.02Z_\odot$ abundances are shown on the top and bottom panels in Fig. 7. Here the solid, dotted and dashed lines display critical star formation efficiencies for $10^5 M_\odot$, $10^6 M_\odot$ and $10^7 M_\odot$ clusters, respectively. The

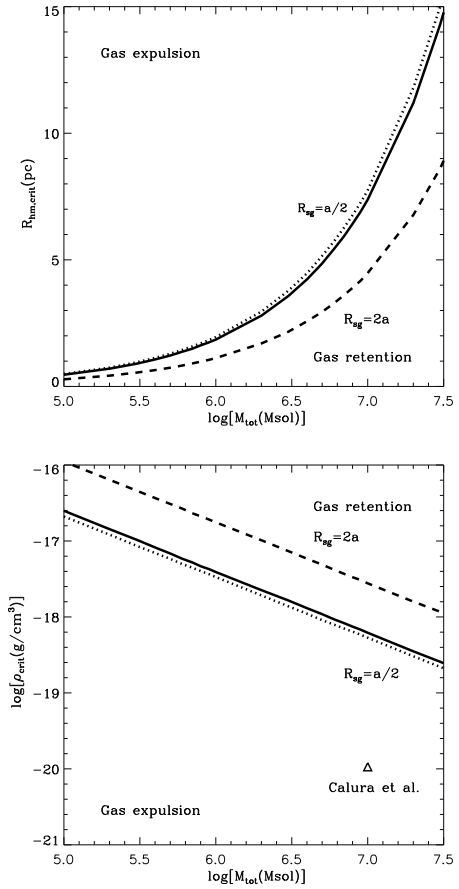


Figure 6. Critical lines for clusters with different mass segregation radii. The solid, dotted and dashed lines displays the critical lines derived for clusters with the same metallicity ($Z = 0.02Z_\odot$) and the star formation efficiency ($\epsilon = 0.3$) but different mass segregation radii: $R_{sg} = a$, $R_{sg} = a/2$ and $R_{sg} = 2a$, respectively.

star formation efficiency must be smaller than the critical one if 1G stars are to avoid forming global wind and the star cluster retains the leftover gas and the reinserted matter. One can note that less massive clusters with a wide spread of compactness index and very high star formation efficiencies may retain the residual gas. In such clusters the stellar feedback is ineffective and they essentially evolve in the gas exhaustion regime discussed in (Ginsburg et al. 2016; Longmore et al. 2014).

5 CONCLUSIONS

Strong negative feedback from massive stars is usually suggested to be responsible for expelling the residual gas and terminating star formation in young stellar clusters. Here we show that negative stellar feedback, which leads to the star-forming cloud destruction, is strongly suppressed in massive and compact star-forming regions. The critical half-mass radii and gas central densities which separate clusters evolving in the negative and positive feedback regimes are obtained. They depend on the star formation efficiency and metallicity of the star-forming cloud and on the primordial mass segregation in the assembling cluster.

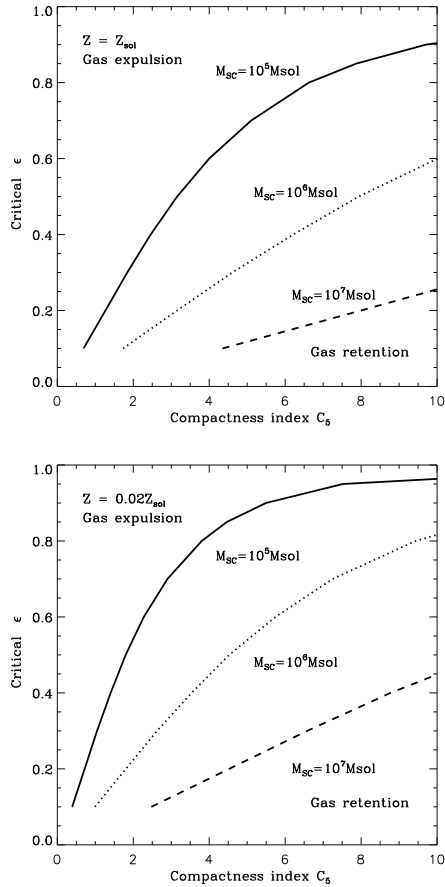


Figure 7. Critical 1G star formation efficiency required for gas retention in young stellar cluster with a given compactness index C_5 . The top and bottom panels present critical star formation efficiencies calculated for clusters with solar and $0.02Z_{sol}$ abundances, respectively. The solid, dotted and dashed lines show critical star formation efficiencies calculated for $10^5 M_{\odot}$, $10^6 M_{\odot}$ and $10^7 M_{\odot}$ clusters, respectively. Clusters with a given compactness index C_5 retain gas if the star formation efficiency in a star-forming cloud is smaller than the critical value. The global wind is formed, the leftover and the reinserted gas are expelled from the cluster if the star formation efficiency is larger than the critical one. The calculations were provided for low metallicity ($Z = 0.02Z_{\odot}$) clusters with $R_{sg} = a$.

In clusters with a negative stellar feedback individual shocked winds merge to form star cluster winds, clear star-forming regions and terminate star formation in a short time-scale. The further star formation in such clusters is possible only after all massive stars from the 1G terminate their life cycle and requires the ambient interstellar medium to be accreted at later stages of their evolution.

In clusters with a positive star formation feedback hot shocked winds around individual massive stars cool before merging with their neighbors. Such clusters do not form hot star cluster winds which expel gas from their parental clouds. They are invisible in the optical or UV emission being deeply embedded into their dense molecular, partially ionized clouds and a system of dense clumps containing thermally unstable processed matter. Such deeply embedded clusters should be detected due to their powerful radio-

continuum and IR radiation coincident with the molecular gas emission as it is the case in the NGC5253 supernova (Turner et al. 2000; Gorjian et al. 2001; Turner et al. 2003; Beck et al. 2012; Beck 2015; Turner et al. 2015). It is likely that in such clusters further generations of stars with different chemical abundances to be formed.

The window of opportunity for clusters to retain gas and form a second stellar population is larger when they develop in clouds with low abundances. In this case less compact clusters formed in less dense proto-cluster clouds may evolve in the positive star formation regime.

It is remarkable that the model-predicted half-mass radii which separate clusters evolving in the negative and positive star-formation regimes are similar to those of globular clusters. Small sizes and high central densities required for the gas retention and secondary star formation suggest that clusters with a positive star formation feedback are formed in a high pressure environment. Such conditions together with low abundances favor early assembling galaxies to be the nests of present-day globular clusters with multiple stellar populations.

ACKNOWLEDGMENTS

The authors thank S. Cassisi for his comments regarding the low mass limit for globular clusters with multiple stellar populations and their anonymous referee for a detailed report full of suggestions which have largely improved the presentation of their results.

REFERENCES

- Adams S. M., Kochanek C. S., Gerke J. R., Stanek K. Z., Dai X., 2017a, *MNRAS*, **468**, 4968
- Adams S. M., Kochanek C. S., Gerke J. R., Stanek K. Z., 2017b, *MNRAS*, **469**, 1445
- Ashman K. M., Zepf S. E., 2001, *AJ*, **122**, 1888
- Bastian N., Lamers H. J. G. L. M., de Mink S. E., Longmore S. N., Goodwin S. P., Gieles M., 2013, *MNRAS*, **436**, 2398
- Baumgardt H., De Marchi G., Kroupa P., 2008, *ApJ*, **685**, 247
- Beck S., 2015, *International Journal of Modern Physics D*, **24**, 1530002
- Beck S. C., Lacy J. H., Turner J. L., Kruger A., Richter M., Crosthwaite L. P., 2012, *ApJ*, **755**, 59
- Bedin L. R., Piotto G., Anderson J., Cassisi S., King I. R., Momany Y., Carraro G., 2004, *ApJ Lett*, **605**, L125
- Cabrera-Ziri I., et al., 2015, *MNRAS*, **448**, 2224
- Calura F., Few C. G., Romano D., D’Ercole A., 2015, *ApJ Lett*, **814**, L14
- Calzetti D., et al., 2015, *ApJ*, **811**, 75
- Carretta E., et al., 2009, *A&A*, **505**, 117
- Carretta E., Bragaglia A., Gratton R. G., Recio-Blanco A., Lucatello S., D’Orazi V., Cassisi S., 2010, *A&A*, **516**, A55
- Cassisi S., Salaris M., 2014, *A&A*, **563**, A10
- Chevalier R. A., Clegg A. W., 1985, *Nature*, **317**, 44
- Conroy C., Spergel D. N., 2011, *ApJ*, **726**, 36
- Consiglio S. M., Turner J. L., Beck S., Meier D. S., 2016, *ApJ Lett*, **833**, L6
- Consiglio S. M., Turner J. L., Beck S., Meier D. S., Silich S., Zhao J.-H., 2017, *ApJ*, **850**, 54
- D’Ercole A., Vesperini E., D’Antona F., McMillan S. L. W., Recchi S., 2008, *MNRAS*, **391**, 825

D’Ercole A., D’Antona F., Ventura P., Vesperini E., McMillan S. L. W., 2010, *MNRAS*, **407**, 854

Decressin T., Meynet G., Charbonnel C., Prantzos N., Ekström S., 2007, *A&A*, **464**, 1029

Decressin T., Baumgardt H., Charbonnel C., Kroupa P., 2010, *A&A*, **516**, A73

Dib S., Shadmehri M., Gopinathan M., Kim J., Henning T., 2008, in Beuther H., Linz H., Henning T., eds, *Astronomical Society of the Pacific Conference Series Vol. 387, Massive Star Formation: Observations Confront Theory*. p. 282 ([arXiv:0710.3969](https://arxiv.org/abs/0710.3969))

Elmegreen B. G., 2017, *ApJ*, **836**, 80

Elmegreen B. G., Efremov Y. N., 1997, *ApJ*, **480**, 235

Ginsburg A., et al., 2016, *A&A*, **595**, A27

Gorjian V., Turner J. L., Beck S. C., 2001, *ApJ Let*, **554**, L29

Gratton R., Sneden C., Carretta E., 2004, *ARA&A*, **42**, 385

Johnson K. E., Leroy A. K., Indebetouw R., Brogan C. L., Whitmore B. C., Hibbard J., Sheth K., Evans A. S., 2015, *ApJ*, **806**, 35

Krause M., Charbonnel C., Decressin T., Meynet G., Prantzos N., Diehl R., 2012, *A&A*, **546**, L5

Krause M. G. H., Charbonnel C., Bastian N., Diehl R., 2016, *A&A*, **587**, A53

Kroupa P., Aarseth S., Hurley J., 2001, *MNRAS*, **321**, 699

Leitherer C., et al., 1999, *ApJS*, **123**, 3

Longmore S. N., et al., 2014, *Protostars and Planets VI*, pp 291–314

Marino A. F., Villanova S., Piotto G., Milone A. P., Momany Y., Bedin L. R., Medling A. M., 2008, *A&A*, **490**, 625

Martín-Hernández N. L., Schaerer D., Sauvage M., 2005, *A&A*, **429**, 449

Massari D., et al., 2017, *MNRAS*, **468**, 1249

Matzner C. D., Jumper P. H., 2015, *ApJ*, **815**, 68

Mirabel F., 2017a, *New Astron. Rev.*, **78**, 1

Mirabel I. F., 2017b, in Gomboc A., ed., *IAU Symposium Vol. 324, New Frontiers in Black Hole Astrophysics*. pp 303–306 ([arXiv:1611.09266](https://arxiv.org/abs/1611.09266)), doi:10.1017/S1743921316012904

Mucciarelli A., et al., 2016, *ApJ*, **824**, 73

Oey M. S., Herrera C. N., Silich S., Reiter M., James B. L., Jaskot A. E., Micheva G., 2017, *ApJ Let*, **849**, L1

Piotto G., et al., 2012, *ApJ*, **760**, 39

Prantzos N., Charbonnel C., 2006, *A&A*, **458**, 135

Rathborne J. M., et al., 2015, *ApJ*, **802**, 125

Raymond J. C., Cox D. P., Smith B. W., 1976, *ApJ*, **204**, 290

Renzini A., 2013, *Mem. Soc. Astron. Italiana*, **84**, 162

Renzini A., et al., 2015, *MNRAS*, **454**, 4197

Salinas R., Strader J., 2015, *ApJ*, **809**, 169

Silich S., Tenorio-Tagle G., 2017, *MNRAS*, **465**, 1375

Silich S., Tenorio-Tagle G., Rodríguez-González A., 2004, *ApJ*, **610**, 226

Silich S., Tenorio-Tagle G., Muñoz-Tuñón C., 2007, *ApJ*, **669**, 952

Smith L. J., Westmoquette M. S., Gallagher J. S., O’Connell R. W., Rosario D. J., de Grijs R., 2006, *MNRAS*, **370**, 513

Smith L. J., Crowther P. A., Calzetti D., Sidoli F., 2016, *ApJ*, **823**, 38

Tenorio-Tagle G., Muñoz-Tuñón C., Silich S., Cassisi S., 2015, *ApJ Let*, **814**, L8

Turner J. L., Beck S. C., Ho P. T. P., 2000, *ApJ Let*, **532**, L109

Turner J. L., Beck S. C., Crosthwaite L. P., Larkin J. E., McLean I. S., Meier D. S., 2003, *Nature*, **423**, 621

Turner J. L., Beck S. C., Benford D. J., Consiglio S. M., Ho P. T. P., Kovács A., Meier D. S., Zhao J.-H., 2015, *Nature*, **519**, 331

Turner J. L., Consiglio S. M., Beck S. C., Goss W. M., Ho P. T. P., Meier D. S., Silich S., Zhao J.-H., 2017, *ApJ*, **846**, 73

Whitmore B. C., et al., 2014, *ApJ*, **795**, 156

Wünsch R., Palouš J., Tenorio-Tagle G., Silich S., 2009, *Ap&SS*, **324**, 219

Wünsch R., Palouš J., Tenorio-Tagle G., Ehlerová S., 2017, *ApJ*, **835**, 60

de Mink S. E., Pols O. R., Langer N., Izzard R. G., 2009, *A&A*, **507**, L1

APPENDIX A: SUBSONIC GROWTH OF A HOT SHOCKED ZONE

Hot, shocked wind zones continue to grow even after the gas pressure drops to that in the turbulent ambient medium and the wind-driven leading shock vanishes, as their central stars continue to deposit mass and energy via their stellar winds. The shocked wind zone grows then in a sub-sonic regime remaining in an approximate pressure equilibrium with the ambient intra-cloud medium. As the velocity of the shocked gas is much smaller than its sound speed (see Fig. 3), one can consider only the shocked wind thermal energy. The subsonic growth of the shocked wind zone is determined then by the following set of equations:

$$\frac{dE_{th}}{dt} = L_* - 4\pi PuR^2, \quad (\text{A1})$$

$$u = \frac{dR}{dt}, \quad (\text{A2})$$

$$E_{th} = \frac{4\pi P}{3(\gamma - 1)} R^3, \quad (\text{A3})$$

$$P = P_g, \quad (\text{A4})$$

where E_{th} , R and u are the thermal energy, radius and growth velocity of the shocked wind zone, respectively. P_g is the intra-cloud gas pressure, which is determined by equation (5) and $L_*(t)$ is a stellar wind mechanical power determined in section 2.2. Because mean separations between neighboring stars and radii of the shocked wind zones are small, one can adopt that the confining pressure P_g does not change as the shocked wind zone grows up. The thermal energy E_{th} and the shocked zone growth velocity u could be eliminated from the set of equations (A1)-(A3) yielding:

$$\frac{dR}{dt} = \frac{(\gamma - 1)L_*(t)}{4\pi\gamma P_t} R^{-2}. \quad (\text{A5})$$

The initial conditions to solve this equations are: $R(t_0) = R_{stall}$, $t_0 = \tau_{stall}$, where the wind-driven shell stalling radius R_{stall} and stalling time τ_{stall} are:

$$R_{stall} = \left(\frac{14a^2}{25G}\right)^{3/4} \left(\frac{3a^3}{M_{tot}^5}\right)^{1/4} \left[\frac{375(\gamma - 1)L_*}{7(9\gamma - 4)(1 - \epsilon)}\right]^{1/2} \times \left(1 + \frac{r^2}{a^2}\right)^{13/8}, \quad (\text{A6})$$

$$\tau_{stall} = \frac{R_{stall}}{a} \left[\frac{7(9\gamma - 4)(1 - \epsilon)M_{tot}R_{stall}^2}{125(\gamma - 1)L_*}\right]^{1/3} \times \left(1 + \frac{r^2}{a^2}\right)^{-5/6}. \quad (\text{A7})$$

One can solve equation (A5) numerically by making use the wind-driven shell stalling time and stalling radius as the initial conditions for the numerical integration. Note, that in

the case of a constant mechanical luminosity, equation (A5) has an analytic solution:

$$R(t) = R_{stall} \left(1 + \frac{t}{\tau_0} \right)^{1/3}, \quad (\text{A8})$$

where t is the time since the wind-driven shell stalls and

$$\tau_0 = \frac{4\pi\gamma P_g R_{stall}^3}{3(\gamma - 1)L_\star}. \quad (\text{A9})$$

This paper has been typeset from a $\text{\TeX}/\text{\LaTeX}$ file prepared by the author.

